Northern Hemisphere summer monsoon intensified by mega-El Niño/southern oscillation and Atlantic multidecadal oscillation

Bin Wang[a,b,1], Jian Liu[c,d], Hyung-Jin Kim[e], Peter J. Webster[f], So-Young Yim[b], and Baoqiang Xiang[b]

[a]Department of Meteorology and [b]International Pacific Research Center, University of Hawaii at Manoa, Honolulu, HI 96822; [c]Key Laboratory of Virtual Geographic Environment of Ministry of Education, Nanjing Normal University, Nanjing 210046, China; [d]State Key Laboratory of Lake Science and Environment, Nanjing Institute of Geography and Limnology, Chinese Academy of Science, Nanjing 210008, China; [e]Research Institute for Global Change, Japan Agency for Marine–Earth Science and Technology, Yokohama, Kanagawa 236-0001, Japan; and [f]School of Earth and Atmospheric Sciences, Georgia Institute of Technology, Atlanta, GA 30308

Prediction of monsoon changes in the coming decades is important for infrastructure planning and sustainable economic development. The decadal prediction involves both natural decadal variability and anthropogenic forcing. Hitherto, the causes of the decadal variability of Northern Hemisphere summer monsoon (NHSM) are largely unknown because the monsoons over Asia, West Africa, and North America have been studied primarily on a regional basis, which is unable to identify coherent decadal changes and the overriding controls on planetary scales. Here, we show that, during the recent global warming of about 0.4 °C since the late 1970s, a coherent decadal change of precipitation and circulation emerges in the entirety of the NHSM system. Surprisingly, the NHSM as well as the Hadley and Walker circulations have all shown substantial intensification, with a striking increase of NHSM rainfall by 9.5% per degree of global warming. This is unexpected from recent theoretical prediction and model projections of the 21st century. The intensification is primarily attributed to a mega-El Niño/Southern Oscillation (a leading mode of interannual-to-interdecadal variation of global sea surface temperature) and the Atlantic Multidecadal Oscillation, and further influenced by hemispherical asymmetric global warming. These factors driving the present changes of the NHSM system are instrumental for understanding and predicting future decadal changes and determining the proportions of climate change that are attributable to anthropogenic effects and long-term internal variability in the complex climate system.

Prediction of monsoon rainfall change in the coming decades is a great challenge because this change involves internal natural variability and external natural (e.g., solar and volcanic activity) and anthropogenic (e.g., greenhouse gas, aerosols, and land use) climate forcings. The global mean surface air temperature has increased by about 0.4 °C since the late 1970s, which accounts for about 50% of the total temperature increase since 1880 (Fig. S1). This accelerated warming is unprecedented in the instrumental record, which, along with the available global observations of monsoon precipitation, provides a unique opportunity for understanding fundamental drivers of the monsoon decadal change with global warming.

The Northern Hemisphere (NH) regional monsoons, including South Asian, East Asian–western North Pacific, West African, and North American monsoons (Fig. 1), encompass about 60% of the population of the planet and, phenomenologically, have profound effects on global climate. Their variability has been extensively studied but mainly on a regional scale (1–4). This regional approach makes some sense as each regional monsoon has indigenous characteristics resulting from different land–ocean configurations. However, decadal variations and the response to external forcing often occur beyond regional scales, and a regional approach is unable to identify overriding and planetary-scale controls. Some recent studies of global-scale monsoon have considered precipitation only (5, 6), yet the results have to be interpreted guardedly as large discrepancies exist between different satellite estimations of oceanic monsoon rainfall (Fig. S2). Such differences may compromise evidence of a trend. Given the uncertainty associated with precipitation-only analyses and the complexity of monsoon dynamics, we carry out an integrated study of the changes of the NH summer monsoon (NHSM) system, which is defined as coherent changes of monsoon precipitation and circulation.

Coherent Variations of the NHSM Precipitation and Circulation

The interannual variation of NHSM rainfall exhibits a largely cohesive pattern with a principal component that is highly correlated with the El Niño/Southern Oscillation (ENSO) index measured by the Niño-3.4 sea surface temperature (SST) anomalies ($r = 0.86$; Fig. S3A), inferring that ENSO exerts a predominant influence. At periods longer than the 3- to 5-y ENSO, the NHSM rainfall displays a coherent increasing trend evident across most regional monsoon areas (Fig. S3B). Given this spatial and temporal coherence, it is possible to measure the NHSM variability by using a combination of the total amount of monsoon rainfall and integrated circulation characteristics.

The overall NHSM rainfall intensity can be measured by the summer mean precipitation rate averaged over the entire NH monsoon domain (7). Here, the NH summer is defined from May to September because the NH rainy season typically begins in May before petering out in September. To detect the long-term variability of the NHSM, it is helpful to establish a circulation index that can reflect the annual reversal of winds and have consistent variability with rainfall. Because a strong monsoon circulation is marked by a strengthening of the vertical zonal wind shear (8), we define a NHSM circulation index by the vertical shear of zonal winds between 850 and 200 hPa averaged in a zone stretching from Mexico eastward to the Philippines (0°–20°N, 120°W–120°E) (Fig. 1C). This region encompasses all of the major NHSM regions and experiences prominent annual reversals of low-level and upper-level zonal winds (Fig. 1 A and B).

This circulation index represents very well the year-to-year variations and overall trends of both the low-level and upper-
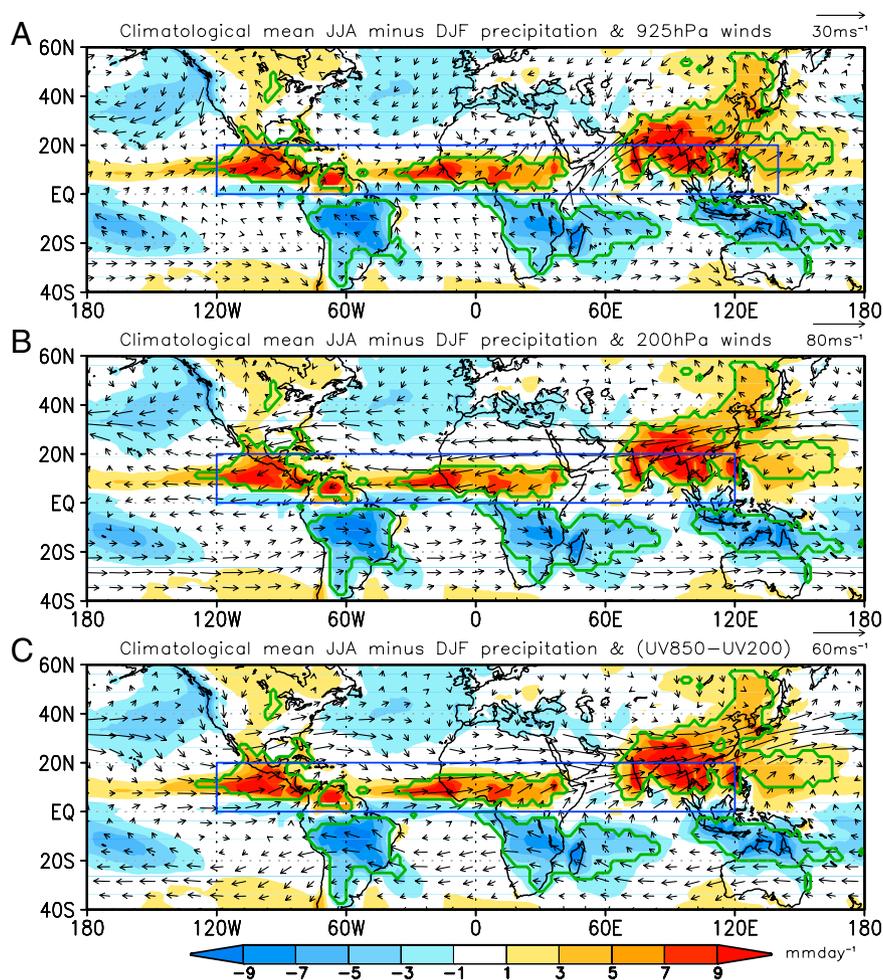
Fig. 1. NH monsoon precipitation domain and annual reversal of the winds. Climatological mean JJA minus DJF rainfall (shading) and (*A*) 925-hPa winds, (*B*) 200-hPa winds, and (*C*) vertical wind shear (VWS, 850-hPa minus 200-hPa winds). The monsoon rainfall domain outlined by the green solid lines is defined by the local summer-minus-winter precipitation rate exceeding 2.0 mm/d and the local summer precipitation exceeding 55% of the annual total (7). The boxed areas in *A*–*C* indicate the regions where the 925 (200)-hPa zonal wind index and NHSM circulation (VWS) index are defined.

level zonal winds (Fig. S4), suggesting that it represents the variation of the 3D NHSM circulation. The circulation index is also highly correlated with the NHSM rainfall intensity (*r* = 0.85 for 1979–2011). The coherent relationship between the NHSM precipitation and circulation indices is well understood through basic dynamics (9, 10), so that such a circulation index is well founded and able to represent the variability of the entire NHSM system.

Substantial Intensification of the NHSM and Tropical Circulation During the Recent Warming Period

Fig. 2*A* shows that, during 1979–2011 (the period for which global precipitation is available), the NHSM rainfall exhibits a significant positive trend of ~0.08 mm·d^{-1} per decade (Table 1) or 9.5% increase per degree of global surface air temperature increase. Consistent with the NHSM precipitation, the NHSM circulation index also shows coherent year-to-year variations and a consistent trend (Fig. 2*B*), indicating that the entire NHSM system has significantly intensified over the recent three decades. However, the multimodel mean projection made by five selected models participated in the phase 5 of the Coupled Model Intercomparison Project (CMIP5) (11) shows a weakening of NHSM circulation trend for 2006–2010 under the RCP4.5 scenario of increasing anthropogenic forcing (Fig. S5), suggesting that the recent intensification of the NHSM system

may arise primarily from internal feedback processes within the climate system rather than from the external forcing such as the increasing greenhouse gases.

The NHSM system is tightly coupled with both the Hadley and Walker circulations (1, 12). However, detecting a trend of Hadley circulation in boreal summer is challenging because regional summer monsoons generate enormous longitudinal variations that may obscure the zonal mean overturning circulation. Additionally, the majority of previous studies have focused on changes of the boreal winter Hadley circulation. To date, robust trends in boreal summer Hadley circulation have not been firmly established (13–15).

Simple thermodynamical arguments have suggested that global warming can weaken the mean tropical atmospheric circulation (16, 17). However, over the recent decades of warming, both the Hadley cell and Walker circulation in boreal summer exhibit significant upward trends (Fig. 2 *C* and *D*), at the 99% and 95% confidence level, respectively (Table 1). Here, the intensity of Hadley circulation is measured by the strength of the cross-equatorial cell of the zonal mean meridional mass stream function (14) (Fig. S6), and the Walker cell strength is measured by the 850-hPa zonal wind averaged over the equatorial Pacific (10°S–10°N, 140°E–120°W). The results of the present study are supported by and consistent with recent diagnostic and theoretical studies (18, 19).
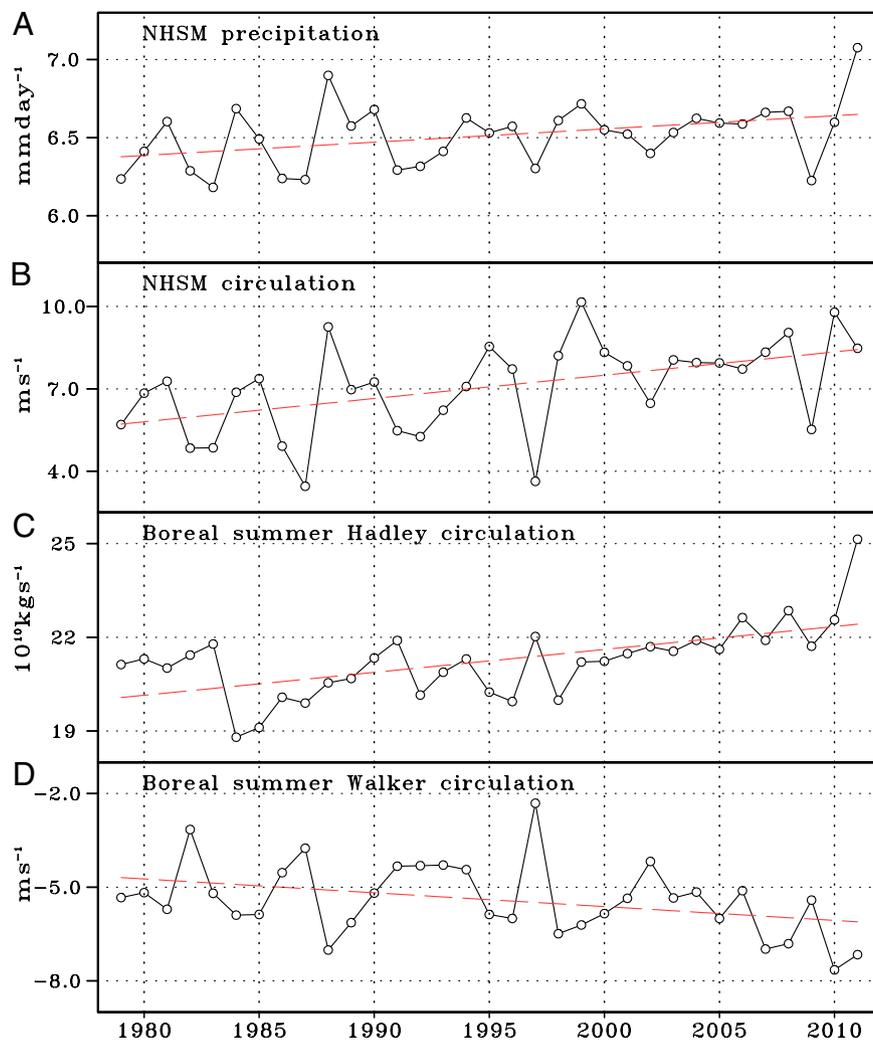
Fig. 2. Variability and trends of the NHSM system, and the Hadley and Walker circulation. Time series of boreal summer (MJJAS) mean indices representing (*A*) NHSM precipitation intensity (mm·d^{-1}) averaged over the entire NH monsoon rainfall domain; (*B*) NHSM circulation intensity measured by the vertical shear of zonal wind (850 hPa minus 200 hPa) averaged over 0°–20°N, 120°W–120°E, which significantly correlates with the NHSM's precipitation index (*r* = 0.85); (*C*) Hadley circulation intensity measured by the maximum absolute value of the cross-equatorial, zonal mean meridional mass stream function (10^{10} kg·s^{-1}); and (*D*) Walker circulation intensity measured by the low-level zonal winds at 850 hPa averaged over the equatorial Pacific (10°S–10°N, 140°E–120°W). The red dashed lines in each panel denote the linear trends, and their statistical significances are shown in Table 1. The ERAI and GPCP, version 2.2, data were used for the period of 1979–2011.

Why Has the NHSM System Intensified?

To understand the origin of the recent trends in NHSM and the tropical circulation, we examine the spatial patterns of lower boundary anomalies associated with the NHSM (Fig. 3). To quantify the characteristic variations of the Pacific SST shown in Fig. 3, we designate the SST difference between the western Pacific K-shape area and eastern Pacific triangle as a "mega-ENSO" index because the spatial pattern shown in Fig. 3 is similar to ENSO but with a larger spatial scale and a longer timescale. The mega-ENSO is a multitimescale index. On the interannual time scale, the mega-ENSO is highly correlated with ENSO index (*r* = 0.91 for 1958–2010) (Fig. S7*A*). However, ENSO has no increasing trend in the past 30 y, whereas mega-ENSO does. Beyond the ENSO time scale, as measured by the 3-y running mean May–September (MJJAS) time series, the mega-ENSO is well correlated with the Pacific Decadal Oscillation (PDO) (20) (*r* = −0.82; Fig. S7*C*). The mega-ENSO has a spatial pattern similar to the ENSO-like interdecadal variability (21) and Interdecadal Pacific Oscillation (IPO) (22, 23).

The IPO was originally defined by the second principal component (PC2) of the 11-y running mean Pacific SST (22). It is very difficult to use this 11-y running definition to study the recent 32-y variation. Thus, in the present study we have modified the original definition of IPO by using the PC2 of the 3-y running mean global SST, which essentially describes a decadal mode of

Table 1. The trends (1979–2011) of the NHSM (MJJAS) precipitation and circulation indices as well as Hadley and Walker circulation intensities shown in Fig. 2 and the mega-ENSO index

1979–2011	Trend (per decade)	TN, %	MK, %
NHSM precipitation intensity	0.08 mm·d^{-1}	98	98
NHSM circulation index	0.85 m·s^{-1}	99	99
Hadley circulation intensity	0.73×10^{10} kg·s^{-1}	99	99
Walker circulation intensity	−0.44 m·s^{-1}	95	95
Mega-ENSO index	0.20 °C	98	99

Also shown are their statistical significance levels by the trend–noise ratio (TN) and Mann–Kendall rank statistics (MK). Area weighting was applied.
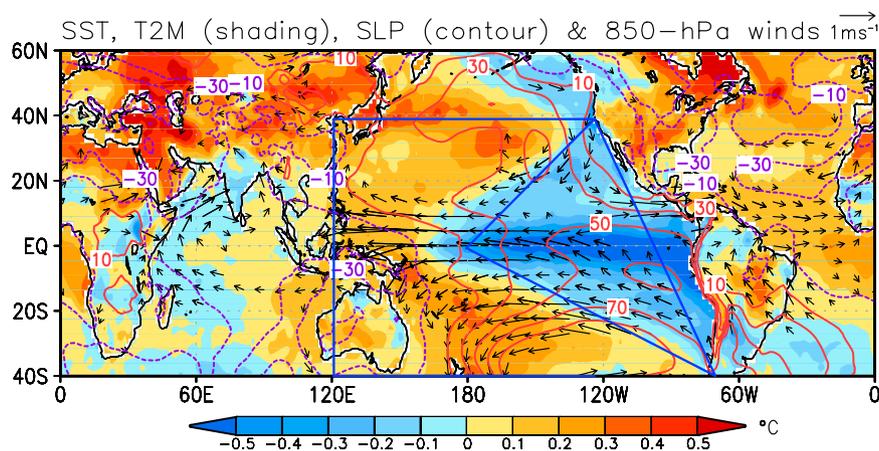
Wang et al.

Fig. 3. Climate anomalies associated with the NHSM circulation index. Regressed 2-m air temperature anomalies over land and SST anomalies over ocean (shading; in degrees Celsius), sea-level pressure anomalies (contours; in pascals) and 850-hPa wind anomalies (vector) with respect to the NHSM circulation (VWS) index for the period of 1979–2010. Wind vectors are significant at 95% confidence level by the Student *t* test. The blue lines outline the eastern Pacific triangle and western Pacific K-shape regions where the mega-ENSO index is defined. The HadISST and ERAI reanalysis data were used.

SST variability (Fig. S8). We have shown that this modified decadal mode can be represented very well by the 3-y running mean mega-ENSO index ($r = 0.97$; Fig. S7B). Thus, the mega-ENSO reflects a broader range of variability than ENSO, PDO, or IPO alone; and it is an integrated measure of the interannual-to-interdecadal variations of the Pacific (or global) SST. Note also that the mega-ENSO is defined by using the total SST filed.

Therefore, the mega-ENSO index is more convenient than the IPO (or any other indices relying on data filtering and/or empirical orthogonal function analysis) for monitoring variations on monthly, seasonal, and annual timescales.

The mega-ENSO has a well-defined spatial structure (Fig. 3) and temporal evolution (Fig. 4). The long-term variation of the NHSM circulation index (1958–2011) is well correlated with the
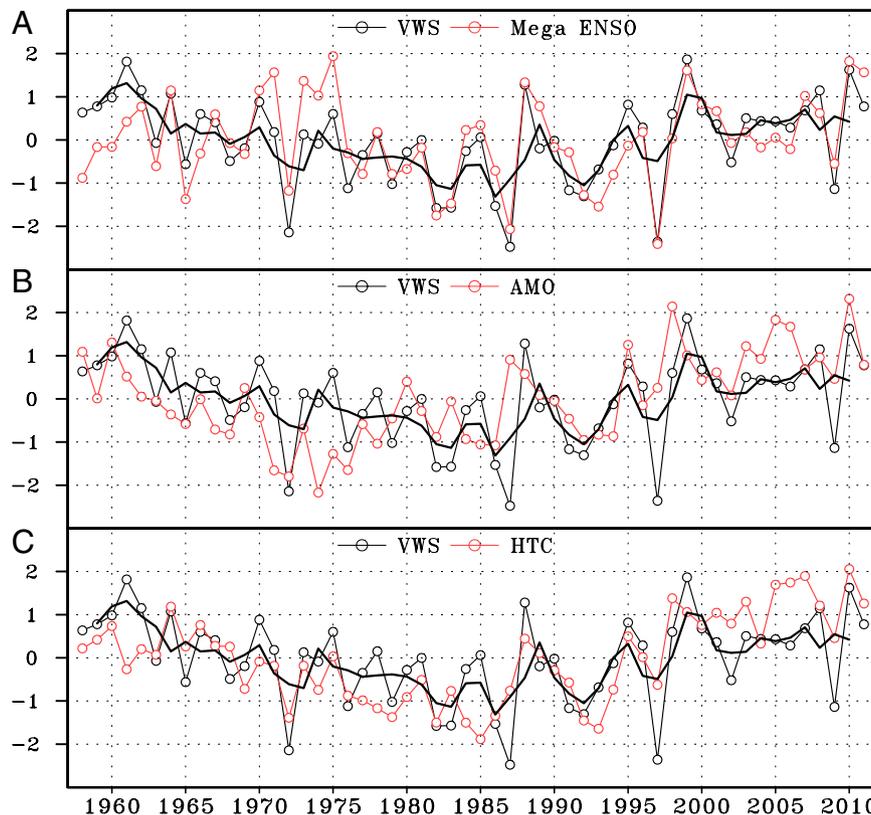

Fig. 4. NHSM circulation index in relation to the mega-ENSO, AMO, and hemispheric thermal contrast (HTC). (*A*) Normalized NHSM circulation index, and the normalized mega-ENSO index ($r = 0.77$). (*B*) Normalized AMO index, which is significantly correlated with the NHSM circulation index ($r = 0.44$). (*C*) Normalized HTC index measured by the 2-m air temperature averaged over the NH (0–60°N) minus that over the SH (0–60°S), which is significantly correlated with the NHSM circulation index ($r = 0.63$). The thick black lines in each panel denote 3-y running means of NHSM circulation index. The merged ERA-40 (1958–1978) and ERAI (1979–2011) reanalysis datasets were used.

Wang et al.

mega-ENSO index ($r = 0.77$; Fig. 4*A*). This significant correlation is confirmed for the period 1871–2010 by using the 20th century reanalysis dataset ($r = 0.62$; Fig. S9). Physically, the eastern Pacific cooling and the western Pacific warming are consistent with a strengthening of the Pacific subtropical highs in the northern and southern hemispheres and their associated trade winds (Fig. 3), causing moisture to converge into the Asian and African monsoon regions and thus contributing to the intensification of NHSM rainfall. Therefore, the recent trend in NHSM is partly driven by mega-ENSO.

We have also found that the NHSM system is significantly linked to the Atlantic Multidecadal Oscillation (AMO) (24) ($r = 0.44$ for 1958–2011), which mainly arises from its decadal variation (Fig. 4*B*). The AMO has been demonstrated to influence some regional monsoon systems over North America, West Africa, and India (25–27). We have further examined the precipitation and wind anomalies associated with AMO on a global scale by regressing the reconstructed precipitation (28) and the 20th century reanalysis winds (29) onto the AMO index from 1900 to 2008 (Fig. S10). The warming in the North Atlantic corresponds to the suppressed rainfall in the tropical central Pacific and easterly anomalies over the western Pacific and westerly anomalies over the rest of the northern tropics (from 120°W to 100°E), which enhances the NHSM. The numerical simulation results obtained with a coupled model (30) are in reasonably good agreement with these observed features (Fig. S11), demonstrating that the AMO-related Atlantic SST anomalies have large impacts on the Pacific SST and the NHSM precipitation and circulation. Note that the AMO is attributed to a natural ocean oscillation (31) and possibly to the volcanic and anthropogenic aerosol emissions (32). The minima of NHSM precipitation and circulation index around 1983 and 1991 reflect the impacts of volcanic eruptions (the El Chichon volcano in March 1982 and Mount Pinatubo in June 1991), as noticed previously (33).

Note also that, with a 3-y running mean, the mega-ENSO and the AMO are independent of each other ($r = 0.07$ for 1958–2011), but both have similar correlations with NHSM circulation index (0.58 and 0.55, respectively) (Fig. 4 *A* and *B*). Therefore, the combined effect of mega-ENSO and AMO, as shown by the multiregression model (0.752 × mega-ENSO + 0.343 × AMO), can explain 73% of the total variance of the NHSM circulation index (i.e., $r = 0.85$ for 1958–2011), suggesting that the recent intensification of the NHSM may be largely due to internal natural variability.

Discussion

Although the mega-ENSO and AMO are primary sources of the interdecadal variations of the NHSM, one cannot rule out the influence of the global warming. Fig. 3 shows that the NH 2-m air temperature has warmed more than the Southern Hemisphere (SH) counterpart by 0.36 °C over the past 32 y. The NHSM intensity is significantly linked to the hemispheric thermal contrast (HTC) defined by the 2-m air temperature difference between the NH (0°–60°N) and Southern Hemisphere (60°S–0°) ($r = 0.63$; Fig. 4*C*). Dynamically, the enhanced hemispheric thermal contrast can generate meridional pressure gradients that drive low-level cross-equatorial flows from the SH to the NH (Fig. 2*C*) and converge into the NHSM trough regions. We note that the "NH warming faster than the SH" or "warm NH–cold SH" pattern is a characteristic of the projected warming under increasing greenhouse gases forcing (5).

There is an increasing demand for decadal climate prediction, which is necessary for infrastructure planning, energy policy, business development, and issues related to sustainability. The results presented here have important ramifications for the prediction of decadal monsoon changes. On this timescale, monsoon climate could be substantially influenced by internal natural variability in the climate system such as mega-ENSO and AMO. The knowledge gained here is also instrumental in determining the proportions of climate change that are attributable to anthropogenic effects and long-term natural variability in the complex climate system.

Methods

Data. We used two global (land and ocean) precipitation datasets available: Global Precipitation Climatology Project (GPCP) (34) and Climate Prediction Center merged analysis of precipitation (CMAP) (35). For detection of interannual variations, an ensemble mean (arithmetic average) of the two datasets was used, but to determine the long-term trend only GPCP data were used because the CMAP is calibrated to atoll gauge data and this calibration may have introduced forged long-term changes (36). Both GPCP and CMAP are not homogeneous over all time due to increase of the satellite observations. However, these data are more homogeneous and reliable over the recent 20 y when a large amount of Special Sensor Microwave/Imager data were used (5). In the present study, the decadal variation is described by a simple low-pass filter, i.e., the 3-y running mean MJJAS time series. The half-point of the response function for this 3-y running mean filter is around 6 y; thus, it largely removes the ENSO signal, which has a periodicity of 2–7 y. A sensitivity test has been made with a 5-y running mean and the results are essentially the same as the 3-y running mean in terms of description of the decadal–interdecadal variations. The interannual variation component can be obtained by subtracting the 3-y running mean from the MJJAS mean time series. The correlation coefficient between the interannual component of ENSO and the interannual component of mega-ENSO is 0.96 for the period of 1958–2010, which is slightly higher than the correlation coefficient (0.91) between the original ENSO and mega-ENSO time series without filtering.

To examine the long-term variability of NHSM, we also use a historical reconstructed precipitation dataset (28) and atmospheric winds from the 20th century reanalysis data (29). The AMO index was downloaded from the website (www.esrl.noaa.gov/psd/data/timeseries/AMO/), which was calculated over the North Atlantic (0°–70°N) using the Kaplan SST data.

The circulation data used are the European Centre for Medium-Range Weather Forecasts (ECMWF) reanalysis (ERA), which includes the 40-y reanalysis (ERA40, 1958–1978) (37) and ERA-Interim (ERAI) reanalysis (1979–2010) (38). The Hadley circulation trends determined from different reanalysis datasets have notorious discrepancies (39, 40). To assess the uncertainties in the Hadley circulation, we have examined four datasets (Fig. S12): ERA40, ERAI reanalysis, National Center for Environmental Prediction (NCEP) reanalysis (NRA1) (41), and NCEP–Department of Energy reanalysis (NRA2) (42). In Figs. 2*C* and 4, we used ERAI reanalysis data (1979–2010). Monthly mean SST data were obtained from the Hadley Centre sea ice and sea surface temperature dataset (HadISST) (43). Two methods are used to test the significance of linear trends: the trend–noise ratio (44) and Mann–Kendall rank statistics (45).

Model and Experiments. To assess future changes of the NHSM (Fig. S5), we selected the top 5 among 20 coupled climate models that participated in CMIP5 and used multimodel mean (MMM) for the historic reconstruction and future projection. The model selection is based on two measures [the pattern correlation coefficient (PCC) and signal-to-noise ratio] of the annual mean precipitation and the combined first and second annual cycles, as well as the global monsoon precipitation intensity (46). We combined the PCCs of the first and second annual cycle mode by weighting with their fractional-variance contributions to the annual variation (i.e., 0.68 and 0.15, respectively). The signal-to-noise ratio is defined by the ratio of the absolute value of the MMM (as a signal) to intermodel standard deviation against the MMM (as a noise) (47). The best five models are ACCESS1, CNRM-CM5, Can-ESM2, HadGEM2-ES, and MIROC5.

To demonstrate impacts of North Atlantic warming on the global precipitation and circulation, we used a coupled model, POP-OASIS-ECHAM model (POEM), which consists of the ECHAM (European Centre Hamburg model, version 4.6) atmospheric model and POP (Parallel Ocean Program, version 2.0.1) ocean model coupled by the Ocean Atmosphere Sea Ice Soil (OASIS, version 3.0) coupler (30). As a common problem of current climate models, the POEM also suffers excessive cold tongue extension and SST warm bias in the southeastern Pacific. We conducted two sets of experiments. The first is a control run, which is freely coupled (20 y), but with a warm SST nudging over the equatorial Pacific and a cold SST nudging over the southeastern Pacific to correct the mean state biases. The other is a sensitivity experiment (20 y), which is the same as the control run but with an

imposed AMO-related warm SST nudging in the Atlantic Ocean (Fig. S11*A*). The ensemble-mean difference between the sensitivity and control experiments is interpreted as the effects of the AMO on the global circulation and precipitation.

1. Webster PJ, et al. (1998) Monsoons: Processes, predictability, and the prospects for prediction. *J Geophys Res* 103(C7):14451–14510.
2. Wang B, Wu R, Lau K-M (2001) Interannual variability of the Asian summer monsoon: Contrasts between the Indian and the Western North Pacific-East Asian monsoons. *J Clim* 14(20):4073–4090.
3. Nicholson SE, Kim E (1997) The relationship of the El Nino Southern oscillation to African rainfall. *Int J Climatol* 17(2):117–135.
4. Higgins RW, Shi W (2000) Dominant factors responsible for interannual variability of the southwest monsoon. *J Clim* 13(4):759–776.
5. Wang B, Liu J, Kim HJ, Webster PJ, Yim SY (2012) Recent changes of the global monsoon precipitation (1979–2008). *Clim Dyn* 39(5):1123–1135, 10.1007/s00382-011-1266-z.
6. Hsu P, Li T, Wang B (2011) Trends in global monsoon area and precipitation over the past 30 years. *Geophys Res Lett* 38:L08701, 10.1029/2011GL046893.
7. Wang B, Ding Q (2008) Global monsoon: Dominant mode of annual variation in the tropics. *Dyn Atmos Oceans* 44(3–4):165–183.
8. Webster PJ, Yang S (1992) Monsoon and ENSO: Selectively interactive systems. *Q J Meteorol Soc* 118(507):877–926.
9. Gill AE (1980) Some simple solutions for heat-induced tropical motion. *Q J R Meteorol Soc* 106(449):447–462.
10. Hoskins B, Wang B (2006) Large scale dynamics. *The Asian Monsoon*, ed Wang B (Springer/Praxis Publishing, New York), pp 357–415.
11. Tayor KE, Stouffer RJ, Meehl GA (2012) An overview of CMIP5 and the experiment design. *Bull Am Meteorol Soc* 93(4):485–498.
12. Trenberth KE, Stepaniak DP, Caron JM (2000) The global monsoon as seen through the divergent atmospheric circulation. *J Clim* 13(22):3969–3993.
13. Tanaka HL, Ishizaki N, Kitoh A (2004) Trend and interannual variability of Walker, monsoon and Hadley circulations defined by velocity potential in the upper troposphere. *Tellus* 56(3):250–269.
14. Quan XW, Diaz HF, Hoerling MP (2004) *Change in the Tropical Hadley Cell Since 1950*, eds Diaz HF, Bradley RS (Cambridge Univ Press, New York), pp 85–120.
15. Mitas CM, Clement A (2005) Has the Hadley cell been strengthening in recent decades? *Geophys Res Lett* 32(3):L03809, 10.1029/2004GL021765.
16. Held IM, Soden BJ (2006) Robust responses of the hydrological cycle to global warming. *J Clim* 19(21):5686–5699.
17. Vecchi GA, et al. (2006) Weakening of tropical Pacific atmospheric circulation due to anthropogenic forcing. *Nature* 441(7089):73–76.
18. Hoyos CD, Webster PJ (2012) Evolution and modulation of tropical heating from the last glacial maximum through the twenty-first century. *Clim Dyn* 38(7–8):1501–1519, 10.1007/s00382-011-1181-3.
19. Nguyen H, Timbal B, Evans A, Lucas C, Smith I (2012) The Hadley circulation in reanalyses: Climatology, variability and change. *J Clim*, 10.1175/JCLI-D-12-00224.1.
20. Mantua NJ, Hare SR, Zhang Y, Wallace JM, Francis RC (1997) A Pacific interdecadal climate oscillation with impacts on salmon production. *Bull Am Meteorol Soc* 78(6):1069–1079.
21. Zhang Y, Wallace JM, Battisti D (1997) ENSO-like interdecadal variability: 1900–93. *J Clim* 10(5):1004–1020.
22. Power S, Casey T, Folland CK, Colman A, Mehta V (1999) Inter-decadal modulation of the impact of ENSO on Australia. *Clim Dyn* 15(5):319–323.
23. Parker D, et al. (2007) Decadal to multidecadal variability and the climate change background. *J Geophys Res* 112(D18):D18115, 10.1029/2007JD00841.
24. Schlesinger ME (1994) An oscillation in the global climate system of period 65–70 years. *Nature* 367(6465):723–726.
25. Zhang R, Delworth TL (2006) Impact of Atlantic multidecadal oscillations on India/Sahel rainfall and Atlantic hurricanes. *Geophys Res Lett* 33(7):L17712, 10.1029/2006GL026267.
26. Hu Q, Feng S, Oglesby RJ (2011) Variations in North American summer precipitation driven by the Atlantic Multidecadal Oscillation. *J Clim* 24(21):5555–5570.
27. Chelliah M, Bell GD (2004) Tropical multidecadal and interannual climate variability in the NCEP–NCAR reanalysis. *J Clim* 17(9):1777–1803.
28. Smith TM, Arkin PA, Ren L, Shen SSP (2012) Improved reconstruction of global precipitation since 1900. *J Atmos Ocean Technol* 29(10):1505–1517.
29. Compo GP, et al. (2011) The twentieth century reanalysis project. *Q J R Meteorol Soc* 137(654):1–28.
30. Xiang B, et al. (2012) Reduction of the thermocline feedback associated with mean SST bias in ENSO simulation. *Clim Dyn* 39(6):1413–1430, 10.1007/s00382-011-1164-4.
31. Knight JR (2009) The Atlantic Multidecadal Oscillation inferred from the forced climate response in coupled general circulation models. *J Clim* 22(7):1610–1625.
32. Booth BBB, Dunstone NJ, Halloran PR, Andrews T, Bellouin N (2012) Aerosols implicated as a prime driver of twentieth-century North Atlantic climate variability. *Nature* 484(7393):228–232, 10.1038/nature10946.
33. Trenberth KE, Dai A (2007) Effects of Mount Pinatubo volcanic eruption on the hydrological cycle as an analog of geoengineering. *Geophys Res Lett* 34(15):L15702.
34. Huffman GJ, Bolvin DT, Adler RF (2011) Global Precipitation Climatology Project, version 2.2, Combined Precipitation Data Set. World Data Center A, National Climatic Data Center, Asheville, NC. Available at www.ncdc.noaa.gov/oa/wmo/wdcamet-ncdc.html. Accessed August 10, 2011.
35. Xie P, Arkin PA (1997) Global precipitation: A 17-y monthly analysis based on gauge observations, satellite estimates, and numerical model outputs. *Bull Am Meteorol Soc* 78(11):2539–2558.
36. Yin P, Gruber A, Arkin P (2004) Comparison of the GPCP and CMAP merged gauge–satellite monthly precipitation products for the period 1979–2001. *J Hydrometeorol* 5(6):1207–1222.
37. Uppala SM, et al. (2005) The ERA-40 re-analysis. *Q J R Meteorol Soc* 131(612):2961–3012.
38. Dee DP, et al. (2011) The ERA-Interim reanalysis: Configuration and performance of the data assimilation system. *Q J R Meteorol Soc* 137(656):553–597.
39. Mitas CM, Clement A (2005) Has the Hadley cell been strengthening in recent decades? *Geophys Res Lett* 32(3), 10.1029/2004GL021765.
40. Mitas CM, Clement A (2006) Recent behavior of the Hadley cell and tropical thermodynamics in climate models and reanalyses. *Geophys Res Lett* 33(1), 10.1029/2005GL024406.
41. Kalnay E, et al. (1996) The NCEP/NCAR 40-Year Reanalysis project. *Bull Am Meteorol Soc* 77(3):437–471.
42. Kanamitsu M, et al. (2002) NCEP-DOE AMIP-II Reanalysis (R-2). *Bull Am Meteorol Soc* 83(11):1631–1643.
43. Rayner NA, et al. (2003) Global analyses of sea surface temperature, sea ice, and night marine air temperature since the late nineteenth century. *J Geophys Res* 108(D14), 10.1029/2002JD002670.
44. Woodward WA, Gray HL (1993) Global warming and the problem of testing for trend in time series data. *J Clim* 6(5):953–962.
45. Kendall MG (1955) *Rank Correlation Methods* (Charles Griffin, London), 2nd Ed, p 160.
46. Wang B, Kim HJ, Kikuchi K, Kitoh A (2011) Diagnostic metrics for evaluation of annual and diurnal cycles. *Clim Dyn* 37(5–6):941–955.
47. Lee J-Y, Wang B (2013) Future change of global monsoon in the CMIP5. *Clim Dyn*, 10.1007/s00382-012-1564-0.